Variable Bandpass Filters Using Varactor Diodes

SACHIHIRO TOYODA, MEMBER, IEEE

Abstract—**A rectangular waveguide type variable bandpass filter for the 4-GHz band has been proposed and tested. The passband width varies from 260 MHz to 1.02 GHz for a filter using varactor diodes. Two microstrip variable bandpass filters for the 6-GHz and 4-GHz bands are also proposed and tested. The passband width varies from 310 MHz to 1.24 GHz for a varactor-diode coupled filter, and it varies from 380 MHz to 2.18 GHz for a filter which is composed of low-pass and high-pass filters connected in cascade. The center frequency of the three filters can be changed arbitrarily.**

I. Introduction

Many studies of microwave filters using rectangular waveguides, coaxial lines, or striplines have been reported. Filters used in a waveguide are usually composed of capacitive or inductive irises placed at quarter-wavelength intervals. Chen [1] obtained wide-band characteristics for a filter composed of resonant irises placed across a rectangular waveguide at quarter-wavelength intervals. However, the passband widths of the bandpass filters mentioned above are fixed and cannot be varied.

In this paper, the author proposes new variable bandpass filters using varactor diodes. The passband width of the filters can be varied mechanically or electrically. These methods of changing the passband width have already been reported by the author *et al.* [2], [3]. Three types of the filters are considered.

The first one is the waveguide type variable bandpass filter. The first pair of diodes and a metallic post separated by $a/3$ in the x-direction are mounted in the upper and lower sides of an E-plane bifurcated waveguide, and other pair of Fig. 1 are placed apart from the first pair by $\lambda_g/4$ in the z-direction.

The second one is a varactor-diode coupled variable bandpass filter which is composed of three parallel resonant circuits connected with varactor diodes and short transmission lines. The center frequencies in the passband of the three resonant circuits are equal, and they are varied by changing the junction capacitances of the varactor diodes. The passband width is varied by changing the capacitances of the varactor diodes.

The third one is composed of low-pass and high-pass filters connected in cascade. The low-pass filter is constructed by mounting three varactor diodes in a microstrip line at a certain interval. By changing the capacitances of the varactor diodes, the cutoff frequency of the low-pass filter is varied. The high-pass filter is constructed by placing three capacitances on a microstrip line, and between them, open transmission lines terminated by varactor diodes are connected as inductances. The cutoff frequency of the filter is varied by changing the capacitances of the varactor diodes. The passband width of the bandpass filter can be varied by changing the capacitances of the varactor diodes in both the low-pass and high-pass filters.

The experiments were carried out at the 4-GHz band. For the third filter, the passband width was varied from 380 MHz to 2.18 GHz. These variable bandpass filters can be used to receive the signal of each channel of the broadcasting satellite, to detect a radar frequency, and so on.

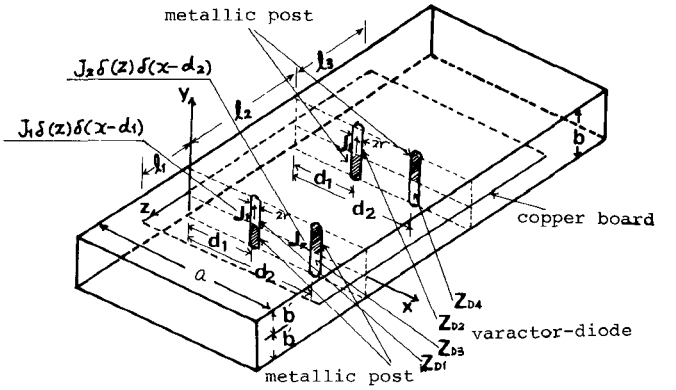

Fig. 1. Variable bandpass filter using varactor diodes and metallic posts mounted in an E-plane bifurcated waveguide.

II. Waveguide Variable Bandpass Filter Using Varactor Diodes

A. Analysis and Equivalent Circuit of the Filter

The structure of variable bandpass filter using the varactor diodes is shown in Fig. 1. The width and height of both upper and lower waveguides are a and b'. Both a diode and a metallic post are assumed to be very thin cylindrical posts of radius r, and are mounted at a distance d_1 and d_2 from the wall in the upper waveguide (the structure of the lower waveguide is the same as that of the upper waveguide). It is assumed that filamentary currents denoted by $J_1\delta(z)\delta(x-d_1)$, $J_2\delta(z)\delta(x-d_2)$ flow uniformly in the posts. The currents J_1 and J_2 are determined from the boundary condition. We consider here the special case

Manuscript received September 3, 1980; revised November 26, 1980.
The author is with the Department of Electrical Engineering, Osaka Institute of Technology, 5-16-1 Omiya, Asahi-ku, Osaka 535, Japan.

0018-9480/81/0400-0356$00.75 ©1981 IEEE

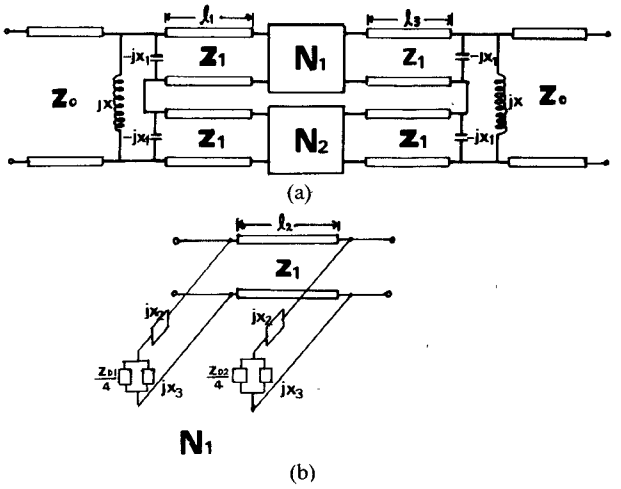

Fig. 2. Equivalent circuit of the filter shown in Fig. 1.

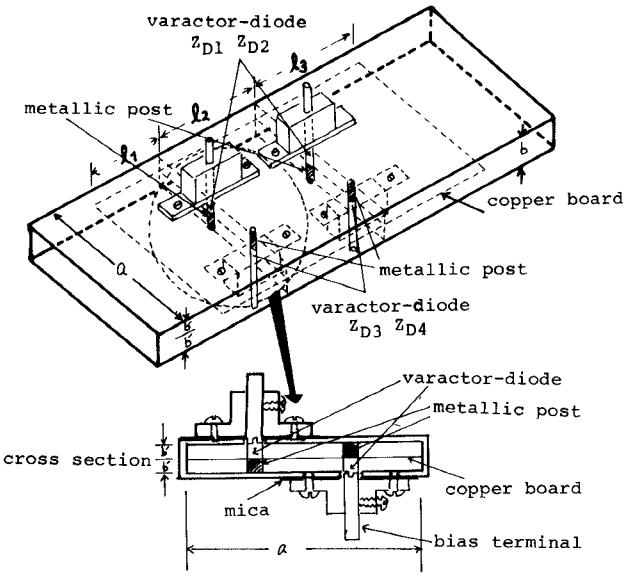

Fig. 3. Structure of the variable bandpass filter shown in Fig. 1.

where the height b' of the waveguide coincides with that of the diode. Since $b' \ll \lambda$ in this case, the electromagnetic field are almost uniform in the y-direction, and therefore the electric field is assumed to have only a y-component $E_y(x, z)$. With these assumptions, the analysis was carried out, and gives the equivalent circuit of the filter shown in Fig. 2 [2]. The equivalent circuit of N_1 in Fig. 2(a) is shown in Fig. 2(b). The equivalent circuit of N_2 is obtained by replacing Z_{D1} and Z_{D2} by Z_{D3} and Z_{D4}, respectively. The expressions for reactances jX, $-jX_1$ are given in [5].

The impedance shown in Fig. 2(b) is expressed as (see the Appendix)

$$Z_s = m^2\left(jX_2 + \frac{1}{\frac{1}{jX_3} + \frac{4}{Z_{D1}}} \right) \tag{1}$$

$$X_2 = \frac{\omega\mu_0 b'}{a} \sum_{n=3,5,7,\cdots}^{\infty} \frac{1}{\Gamma_n} \sin\left(\frac{n\pi d_1}{a}\right) \sin\left\{\frac{n\pi(d_1+r)}{a}\right\} \tag{2}$$

$$X_3 = \frac{\omega\mu_0 b'}{a} \sum_{n=2,4,6,\cdots}^{\infty} \frac{1}{\Gamma_n} \sin\left(\frac{n\pi d_1}{a}\right) \sin\left\{\frac{n\pi(d_1+r)}{a}\right\} \tag{3}$$

$$m^2 = \frac{a}{2b'} \csc^2\left(\frac{\pi d_1}{a}\right). \tag{4}$$

Quantity X_2 in (2) represents the inductive reactance resulting from all the mode components higher than the TE_{10} mode, and the equivalent circuit shows that impedances jX_3 and Z_{D1} of the metallic post and of the diode are connected in series to X_2. m is the transformation ratio of an ideal transformer, and Z_1 and Z_0 are the characteristics impedances of waveguides of height b' and b, respectively.

B. Experimental Results

The structure of the variable bandpass filter is shown in Fig. 3. The values of a, b', and b of the waveguide are 58 mm, 2 mm, and 5 mm, respectively. The thickness of a copper plate is 1 mm. The diameter of the copper post is 3 mm, and the radii r of both the varactor diode and the metallic post are 0.6 mm. The lengths l_1, l_2, l_3 are all $\lambda_g/4$ at a frequency of 4 GHz, and the input power was 0.01 mW.

The measured attenuation characteristics of the variable bandpass filter are shown in Fig. 4. The junction capacitances of varactor diodes Z_{D1}, Z_{D2} and Z_{D3}, Z_{D4} shown in Fig. 4 will be denoted simply as C_1, C_2, and C_3, C_4 in the following. As shown in Fig. 4(a), the passband width varied from 300 MHz to 820 MHz when the bias voltages of the diodes Z_{D3} and Z_{D4} were changed from -0.05 V to -6 V with constant bias voltage of -25 V applied to the diodes Z_{D1} and Z_{D2}. Fig. 4(b) indicates that the passband width varied from 260 MHz to 1.02 GHz when the bias voltages of the diodes Z_{D1} and Z_{D2} were changed from -1 V to -25 V (bias voltage of Z_{D3} and Z_{D4} was varied from -0.3 V to -2.5 V).

When the values of the junction capacitances C_1, C_2 and C_3, C_4 of the varactor diodes are the same, the characteristics of the filters N_1 and N_2 are identical and, therefore, the passband width is very wide as seen from the curve in Fig. 4(b) with $C_1 = C_2 = 0.7$ pF and $C_3 = C_4 = 0.7$ pF. In case of $C_1 = C_2 = 0.8$ pF, $C_3 = C_4 = 1$ pF, the filter N_2 is inductive when N_1 is at resonance. For a frequency higher than the center frequency of N_1, both N_1 and N_2 are inductive. For a frequency lower than the center frequency of N_1, N_1 is capacitive and N_2 is inductive. When the frequency becomes still lower, N_1 is capacitive and N_2 is at resonance. These variation of N_1 and N_2 from inductive to capacitive, and characteristics of $\lambda_g/4$ transmission line and of the discontinuities of an E-plane bifurcated waveguide all contribute to the narrow passband width of the filter when the capacitances C_1, C_2 and C_3, C_4 are not the same.

The experimental results are compared with the theoretical results in Fig. 4(a) and 4(b), and good agreement between them is observed. Moreover, the measured insertion loss in the passband was 0.3 dB (the VSWR in the

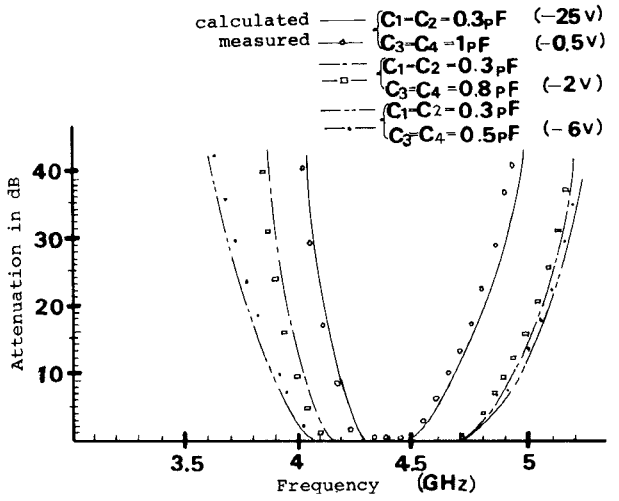

(a)

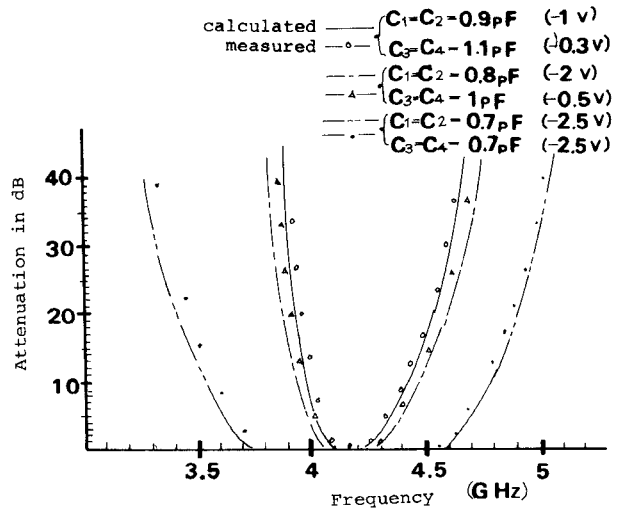

(b)

Fig. 4. Attenuation characteristics of the variable bandpass filter shown in Fig. 1.

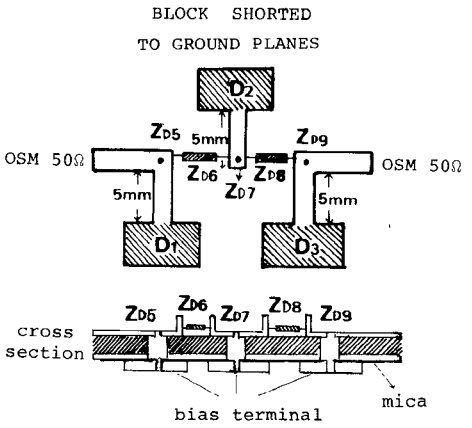

Fig. 5. Varactor-diode coupled variable bandpass filter composed of three resonant circuits connected with varactor diodes and short transmission line.

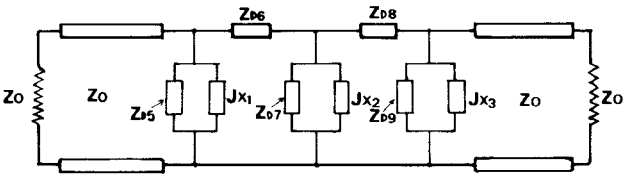

Fig. 6. Equivalent circuit of the filter shown in Fig. 5.

passband varies in the range from 1.2 to 1.3). In order to reduce the insertion loss in the passband, we set the values of C_1 and C_2 equal, and the values of C_3 and C_4 were also made equal. The resonant frequencies in the two resonant circuits are different when the values of C_1 and C_2 are different, and in this case the amount of reflection is large and, therefore the insertion loss in the passband is also large.

If we wish to move the center frequency of the filter to around 3-GHz varactor diodes with larger junction capacitances should be used. According to the analysis, the values of C_1, C_2 and C_3, C_4 are 1.2 pF if the center frequency is 3.4 GHz. The range of the junction capacitance of the varactor diode which can be used in the variable bandpass filter using 4-GHz waveguide is from 0.3 pF to 1.6 pF.

III. Varactor-Diode Coupled Variable Bandpass Filter

The structure of the varactor-diode coupled variable bandpass filter using a microstrip line is shown in Fig. 5. The filter is composed of three resonant circuits connected with varactor diodes and short transmission lines. The center frequencies in the passband of the three resonant circuits are equal, and they varied by changing the junction capacitances of the D5047 varactor diodes Z_{D5}, Z_{D7}, and Z_{D9}. The lengths of the short transmission lines are all 5 mm. In order to supply the voltage to varactor diode, the transmission lines shorted by capacitances D_1, D_2, and D_3 are connected to the stripline. The passband width is varied by changing the capacitances of the varactor diodes Z_{D6} and Z_{D8}. The equivalent circuit of the varactor-diode coupled variable bandpass filter is shown in Fig. 6. J_{x1}, J_{x2} and J_{x3} are the inductances of the short transmission lines. The junction capacitances of the varactor diodes Z_{D5}, Z_{D6}, Z_{D7}, and Z_{D8}, Z_{D9} will be denoted simply as C_5, C_6, C_7, and C_8, C_9 in the following.

The experiments were carried out at the 6-GHz band. The measured attenuation characteristics of the filter is shown in Fig. 7. The input power was 0.01 mW. As shown in Fig. 7(a), the passband width varied from 310 MHz to 1.24 GHz when the bias voltages of the diodes Z_{D6} and Z_{D8} were changed from 0 V to -9.5 V with constant bias voltage of -25 V applied to the diodes Z_{D5}, Z_{D7}, and Z_{D9}. The center frequency is 6.8 GHz. When the junction capacitances of Z_{D6} and Z_{D8} become larger, the coupling between the three resonance circuit increases. As a result, the center frequency is shifted to a lower frequency by 45 MHz.

Fig. 7(b) indicates that the passband width varied from 160 MHz to 1.09 GHz when the bias voltages of the diodes Z_{D6} and Z_{D8} were changed from 0 V to -9.5 V with constant bias voltage -6.2 V applied to the diodes Z_{D5}, Z_{D7}, and Z_{D9}. The center frequency is 6.3 GHz. As shown in Fig. 7(c), the passband width varied from 140 MHz to

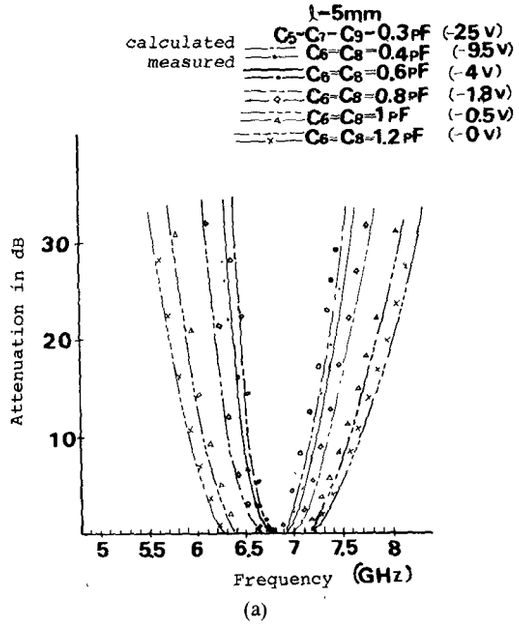

(a)

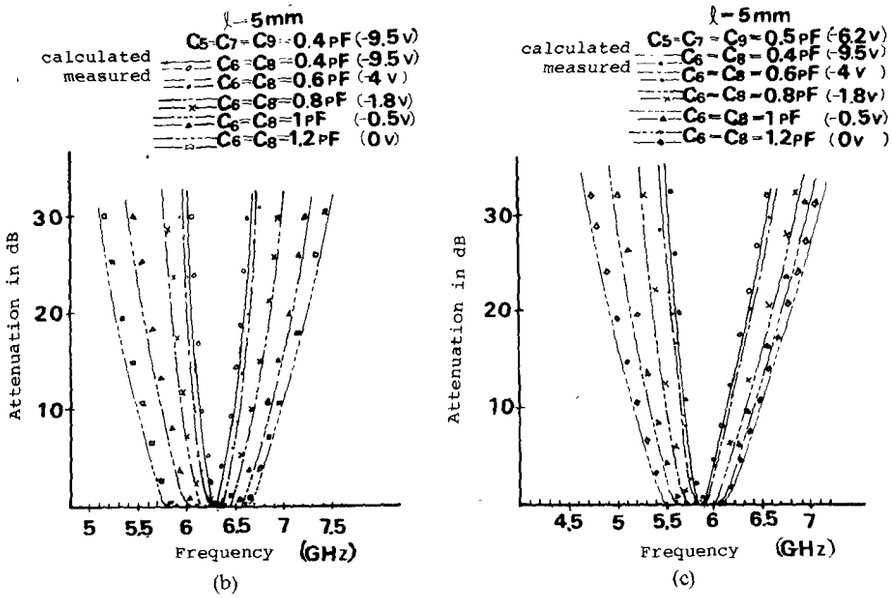

(b) (c)

Fig. 7. Attenuation characteristics of the bandpass filter shown in Fig. 5.

840 MHz when the bias voltage of the diodes Z_{D6} and Z_{D8} was changed from 0 V to −9.5 V with constant bias voltage −6.2 V applied to the diodes Z_{D5}, Z_{D7}, and Z_{D9}. It is seen from Fig. 7 that the center frequencies in the passband varied from 5.8 GHz to 6.8 GHz when the bias voltage of the diodes Z_{D5}, Z_{D7}, and Z_{D9} was changed from −6.2 V to −25 V.

The experimental results are compared with the theoretical results in Fig. 7, and good agreement between them is observed. The measured insertion loss in the passband was 0.4 dB (the VSWR in the passband varies in the range from 1.2 to 1.3).

IV. Variable Bandpass Filter Composed of Low-Pass and High-Pass Filters Connected in Cascade

A. Low-Pass Filter

The structure of the variable cutoff frequency low-pass filter is shown in Fig. 8. The distance between the D5047 varactor diodes Z_{D10}, Z_{D11}, and Z_{D12} is 6 mm, and they are mounted in a microstrip line. As shown in Fig. 8, the input and output impedance of the low-pass filter are 50 Ω, and Z_{01} is 75 Ω. The cutoff frequency in the low-pass filter is varied by changing the capacitances of the varactor diodes.

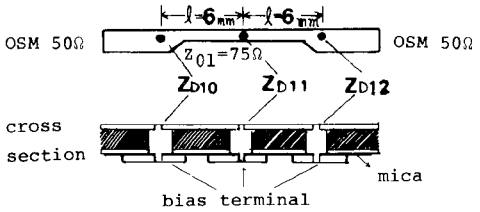

Fig. 8. Low-pass filter constructed by mounting three varactor diodes in a microstrip line.

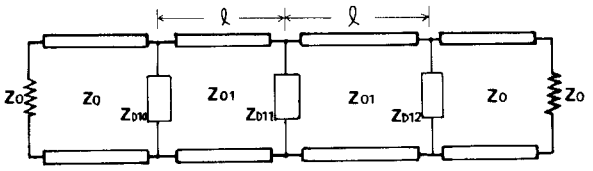

Fig. 9. Equivalent circuit of the filter shown in Fig. 8.

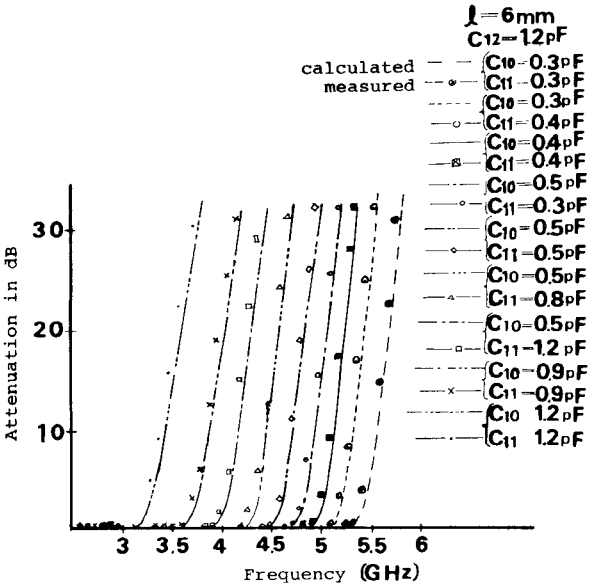

Fig. 10. Attenuation characteristics of the low-pass filter shown in Fig. 8.

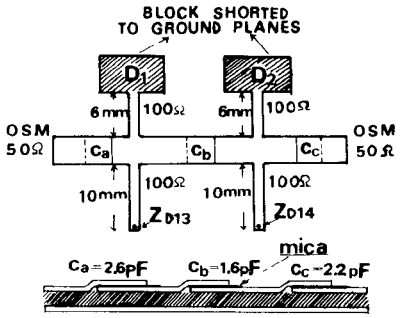

Fig. 11. High-pass filter constructed by placing three capacitances on a microstrip line, and by connecting between them two inductances which consist of open transmission lines terminated by varactor diodes.

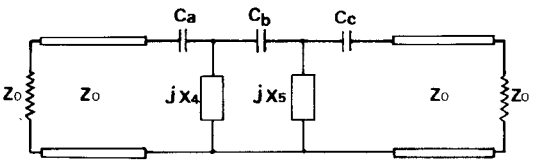

Fig. 12. Equivalent circuit of the filter shown in Fig. 11.

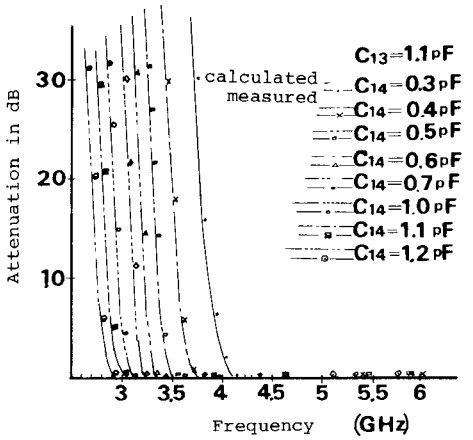

Fig. 13. Attenuation characteristics of the high-pass filter shown in Fig. 11.

The equivalent circuit is shown in Fig. 9. The junction capacitances of the varactor diodes Z_{D10}, Z_{D11}, and Z_{D12} will be denoted simply as C_{10}, C_{11}, and C_{12} in the following.

The measured attenuation characteristics of the variable cutoff frequency low-pass filter are shown in Fig. 10. The cutoff frequency varied from 3.25 GHz to 5.37 GHz when the bias voltage of the diodes Z_{D10} and Z_{D11} was changed from 0 V to −25 V with zero bias voltage applied to the diode Z_{D12}. The experimental results are compared with the theoretical results in Fig. 10, and good agreement is observed.

B. High-Pass Filter

The structure of the variable cutoff frequency high-pass filter is shown in Fig. 11. It is constructed by placing three capacitances on a microstrip line, and between them stube terminated by varactor diodes are connected as inductances. The D5047 varactor diodes Z_{D13} and Z_{D14} are mounted at the ends of the open transmission lines. The characteristics impedance of the open transmission line is 100 Ω, and the length is 10 mm. In order to supply the voltage to the varactor diodes, transmission lines shorted by capacitances D_1 and D_2 are connected to the stripline. The characteristic impedance of the short transmission line is 100 Ω, and the length was 6 mm. The input and output impedances of the high-pass filter are 50 Ω. The capacitances C_a, C_b, and C_c are formed by sandwiching mica plate between the upper and lower plates of the microstrip. The cutoff frequency is varied by changing the capacitances of the varactor diodes. The equivalent circuit of the variable cutoff frequency high-pass filter is shown in Fig. 12. The junction capacitances of the varactor diodes Z_{D13} and Z_{D14} will be denoted simply as C_{13} and C_{14} in the following.

The measured attenuation characteristics of the variable cutoff frequency high-pass filter is shown in Fig. 13. The cutoff frequency varied from 2.86 GHz to 4.05 GHz when

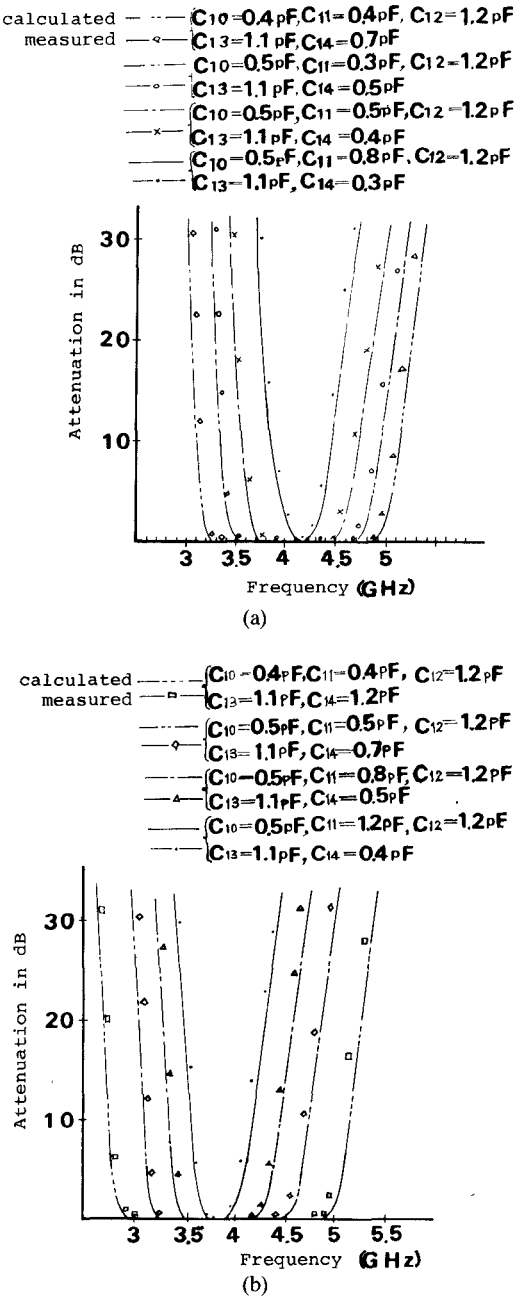

Fig. 14. Variable bandpass filter composed of low-pass and high-pass filters connected in cascade.

the bias voltage of the diode Z_{D14} was changed from 0 V to -25 V with constant bias voltage -0.4 V applied to the diode Z_{D13}. The experimental results are compared with the theoretical results in Fig. 13, and again good agreement is observed.

C. Variable Bandpass Filter Composed of Low-Pass and High-Pass Filter

The measured attenuation characteristics of the variable bandpass filter are shown in Fig. 14. As seen from Fig. 14(a), the passband width varied from 320 MHz to 1.805 GHz when the bias voltage of the diode Z_{D10} was changed from -6.2 V to -9.7 V, that of Z_{D11} was changed from -1.8 V to -9.7 V, and that of Z_{D14} was from -2.6 V to

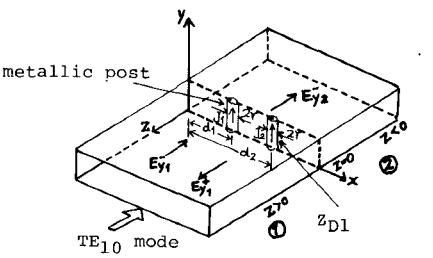

Fig. 15. Rectangular waveguide mounting a diode and a metallic post.

-25 V. In this case, constant bias voltages 0 V and -0.4 V were applied to the diodes Z_{D12} and Z_{D13}, respectively. The center frequency is 4.15 GHz. It is seen from Fig. 14(b) that the passband width varied from 380 MHz to 2.18 GHz when the bias voltage of the diode Z_{D10} was changed from -6.2 V to -9.7 V and those of Z_{D11} and Z_{D14} were changed from 0 V to -9.7 V. In this case constant bias voltages 0 V and -0.4 V were applied to the diodes Z_{D12} and Z_{D13}, respectively. The center frequency is 3.8 GHz.

The experimental results are compared with the theoretical results in Fig. 14, and good agreement between them is observed. Moreover, the measured insertion loss in the passband was 0.3 dB (the VSWR in the passband varies in the range from 1.1 to 1.35). This type of bandpass filter has advantages over the varactor-diode coupled bandpass filter, namely, that center frequency of the passband can be selected more easily, and the passband width can be varied more widely.

V. Conclusion

A rectangular waveguide type variable bandpass filter and two microstrip variable bandpass filters for 6-GHz and 4-GHz bands have been constructed and tested. The passband width varied from 260 MHz to 1.02 GHz in the filter using the rectangular waveguide, and it varied from 380 MHz to 2.18 GHz for the filter which is composed of low-pass and high-pass filters connected in cascade. It was confirmed that the center frequency of three filters could be changed arbitrarily. The experimental results on the attenuation characteristics of the three filters agree well with the theoretical results.

Appendix

We consider here the special case where the height b' of the waveguide coincides with that of the diode. Since $b' \ll \lambda$ in this case, the electromagnetic field are almost uniform in the y-direction.

As seen from Fig. 15 the diode and a metallic post are mounted at the boundary between regions ① and ② in a rectangular waveguide. Using Fourier series expansion of the field, the electric field in each region can be expressed by the following equations:

$$E_{y1}^{-} = A_0 \sin\left(\frac{\pi x}{a}\right) e^{\Gamma_1 z} \tag{A1}$$

$$E_{y1}^{+} = \sum_{n=1}^{\infty} B_n \sin\left(\frac{n\pi x}{a}\right) e^{-\Gamma_n z} \tag{A2}$$

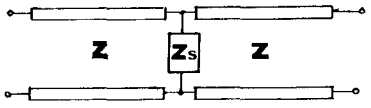

Fig. 16. Equivalent circuit of the waveguide shown in Fig. 15.

$$E_{y2}^{-}=\sum_{n=1}^{\infty} C_n \sin\left(\frac{n\pi x}{a}\right)e^{\Gamma_n z} \tag{A3}$$

where E_{y1}^{-}, E_{y1}^{+}, and E_{y2}^{-} represent the incident, reflected, and transmitted waves, respectively. B_n and C_n are unknown constants and A_0 is the amplitude of the incident wave. Since the electric field must be continuous at $z=0$ we obtain

$$A_0 \sin\left(\frac{\pi x}{a}\right)+\sum_{n=1}^{\infty} B_n \sin\left(\frac{n\pi x}{a}\right)=\sum_{n=1}^{\infty} C_n \sin\left(\frac{n\pi x}{a}\right). \tag{A4}$$

The x-component of the magnetic field in each region can be obtained by substituting (A1), (A2), and (A3) into (A4). Now, it is assumed that the diode and a metallic post are very thin post, and filamentary currents denoted by $J_1\delta(z)\delta(x-d_1)$, $J_2\delta(z)\delta(x-d_2)$ flow uniformly in the post. J_1 and J_2 are determined by the boundary conditions. From the boundary condition for the magnetic field at $z=0$, we have

$$\sum_{n=1}^{\infty}\Gamma_n(-B_n-C_n)\sin\left(\frac{n\pi x}{a}\right)=j\omega\mu_0\{J_1\delta(x-d_1)+J_2\delta(x-d_2)\}-A_0\Gamma_1\sin\left(\frac{\pi x}{a}\right). \tag{A5}$$

Multiplying (A4) and (A5) by $\sin(n\pi x/a)$ and integrating the result from $x=0$ to $x=a$, one can determine the constants B_n and C_n, namely

$$B_1=-j\frac{\omega\mu_0}{a\Gamma_1}\left\{J_1\sin\left(\frac{\pi d_1}{a}\right)+J_2\sin\left(\frac{\pi d_2}{a}\right)\right\} \tag{A6}$$

$$C_1=B_1+A_0 \tag{A7}$$

$$B_n=-j\frac{\omega\mu_0}{a\Gamma_n}\left\{J_1\sin\left(\frac{n\pi d_1}{a}\right)+J_2\sin\left(\frac{n\pi d_2}{a}\right)\right\}, \qquad n\geqslant 2 \tag{A8}$$

$$C_n=B_n, \qquad n\geqslant 2. \tag{A9}$$

The electric field for $z\geqslant 0$ is given by

$$E_{y1}=E_{y1}^{-}+E_{y1}^{+}=A_0\sin\left(\frac{\pi x}{a}\right)e^{\Gamma_1 z}-\sum_{n=1}^{\infty}\frac{j\omega\mu_0}{a\Gamma_n}\cdot\left\{J_1\sin\left(\frac{n\pi d_1}{a}\right)+J_2\sin\left(\frac{n\pi d_2}{a}\right)\right\}\sin\left(\frac{n\pi x}{a}\right)e^{-\Gamma_n z}. \tag{A10}$$

Following the calculation by Lewin [6], it is assumed that electric field is continuous at $z=0$, and at $x=d_1+r$ and $x=d_2-r$. From (A10), the electric fields at the diode and a metallic post are given by

$$0=A_0\sin\left\{\frac{\pi(d_1+r)}{a}\right\}-\sum_{n=1}^{\infty}\frac{j\omega\mu_0}{a\Gamma_n}\cdot\left[J_1\sin\left(\frac{n\pi d_1}{a}\right)-J_2(-1)^n\sin\left(\frac{n\pi d_1}{a}\right)\right]\cdot\left[-(-1)^n\sin\left\{\frac{n\pi(d_1+r)}{a}\right\}\right] \tag{A11a}$$

$$E_{y1}(d_1+r,0)=A_0\sin\left\{\frac{\pi(d_1+r)}{a}\right\}-\sum_{n=1}^{\infty}\frac{j\omega\mu_0}{a\Gamma_n}\left\{J_1\sin\left(\frac{n\pi d_1}{a}\right)-J_2(-1)^n\cdot\sin\left(\frac{n\pi d_1}{a}\right)\right\}\sin\left\{\frac{n\pi(d_1+r)}{a}\right\}. \tag{A11b}$$

The potential difference between lower and upper surfaces of the waveguide is expressed as

$$V_1=-\int_0^{b'}E_{y1}d_y=-b'E_{y1}(d_1+r,0) \tag{A12}$$

$$V_1=Z_{D1}(-J_1). \tag{A13}$$

Substituting (A11a), (A11b), and (A12) into (A13), we obtain

$$J_1\left[Z_{D1}+\sum_{n=1}^{\infty}\frac{j\omega\mu_0 b'}{a\Gamma_n}\sin\left(\frac{n\pi d_1}{a}\right)\sin\left\{\frac{n\pi(d_1+r)}{a}\right\}\right]-J_2\sum_{n=1}^{\infty}\frac{j\omega\mu_0 b'}{a\Gamma_n}(-1)^n\sin\left(\frac{n\pi d_1}{a}\right)\sin\left\{\frac{n\pi(d_1+r)}{a}\right\}=A_0 b'\sin\left\{\frac{\pi(d_1+r)}{a}\right\} \tag{A14a}$$

$$-J_1\sum_{n=1}^{\infty}\frac{j\omega\mu_0}{a\Gamma_n}\sin\left(\frac{n\pi d_1}{a}\right)(-1)^n\sin\left\{\frac{n\pi(d_1+r)}{a}\right\}+J_2\sum_{n=1}^{\infty}\frac{j\omega\mu_0}{a\Gamma_n}(-1)^n\sin\left(\frac{n\pi d_1}{a}\right)(-1)^n\cdot\sin\left\{\frac{n\pi(d_1+r)}{a}\right\}=A_0\sin\left\{\frac{\pi(d_1+r)}{a}\right\} \tag{A14b}$$

where distance d_2 from the waveguide wall to the diode Z_{D1} is denoted by $d_2=a-d_1$.

In general, current densities J_1 and J_2 in the diode and metallic post are different. It can be easily shown that J_1 and J_2 can be expressed in terms of antisymmetric and symmetric components. From (A14a) and (A14b), J_1 and J_2 are calculated as

$$J_1 = \frac{A_0 b' \sin\left\{\frac{\pi(d_1+r)}{a}\right\}\left[\sum_{n=1}^{\infty}\frac{j\omega\mu_0}{a\Gamma_n}\sin\left(\frac{n\pi d_1}{a}\right)\sin\left\{\frac{n\pi(d_1+r)}{a}\right\} + \sum_{n=1}^{\infty}\frac{j\omega\mu_0}{a\Gamma_n}(-1)^n\sin\left(\frac{n\pi d_1}{a}\right)\sin\left\{\frac{n\pi(d_1+r)}{a}\right\}\right]}{Z_{D1}\sum_{n=1}^{\infty}\frac{j\omega\mu_0}{a\Gamma_n}\sin\left(\frac{n\pi d_1}{a}\right)\sin\left\{\frac{n\pi(d_1+r)}{a}\right\} + 4b'\sum_{n=1,3,5\cdots}^{\infty}\frac{j\omega\mu_0}{a\Gamma_n}\sin\left(\frac{n\pi d_1}{a}\right)\sin\left\{\frac{n\pi(d_1+r)}{a}\right\} \cdot \sum_{n=2,4,6,\cdots}^{\infty}\frac{j\omega\mu_0}{a\Gamma_n}\sin\left(\frac{n\pi d_1}{a}\right)\sin\left\{\frac{n\pi(d_1+r)}{a}\right\}} \tag{A15a}$$

$$J_2 = \frac{A_0 \sin\left\{\frac{\pi(d_1+r)}{a}\right\}\left[Z_{D1} + \sum_{n=1}^{\infty}\frac{j\omega\mu_0 b'}{a\Gamma_n}\sin\left(\frac{n\pi d_1}{a}\right)\sin\left\{\frac{n\pi(d_1+r)}{a}\right\} + \sum_{n=1}^{\infty}\frac{j\omega\mu_0 b'}{a\Gamma_n}\sin\left(\frac{n\pi d_1}{a}\right)(-1)^n\sin\left\{\frac{n\pi(d_1+r)}{a}\right\}\right]}{Z_{D1}\sum_{n=1}^{\infty}\frac{j\omega\mu_0}{a\Gamma_n}\sin\left(\frac{n\pi d_1}{a}\right)\sin\left\{\frac{n\pi(d_1+r)}{a}\right\} + 4b'\sum_{n=1,3,\cdots}^{\infty}\frac{j\omega\mu_0}{a\Gamma_n}\sin\left(\frac{n\pi d_1}{a}\right)\sin\left\{\frac{n\pi(d_1+r)}{a}\right\} \cdot \sum_{n=2,4,6,\cdots}^{\infty}\frac{j\omega\mu_0}{a\Gamma_n}\sin\left(\frac{n\pi d_1}{a}\right)\sin\left\{\frac{n\pi(d_1+r)}{a}\right\}.} \tag{A15b}$$

Now, the equivalent circuit such as that shown in Fig. 16 is assumed. In Fig. 16, Z indicates the mode impedance, and is given by

$$Z = \frac{j\omega\mu_0}{\Gamma_1}. \tag{A16}$$

The impedance Z_s represents the total equivalent impedance of the diode and metallic post mentioned above. The voltage reflection coefficient R of the fundamental mode at $z=0$ is given by

$$R = \frac{\frac{Z_s}{Z} - \left(1+\frac{Z_s}{Z}\right)}{\frac{Z_s}{Z} + \left(1-\frac{Z_s}{Z}\right)}. \tag{A17}$$

Hence, we obtain

$$\frac{Z_s}{Z} = \frac{-(1+R)}{2R}. \tag{A18}$$

From (A10), R is given by

$$R = \left\{\frac{-j\omega\mu_0(J_1+J_2)\sin\left(\frac{\pi d_1}{a}\right)}{A_0 a\Gamma_1}\right\}. \tag{A19}$$

Substituting (A19) into (A18), we obtain

$$Z_s = \frac{A_0 a}{2(J_1+J_2)\sin\left(\frac{\pi d_1}{a}\right)} - \frac{Z}{2} = m^2\left(jX_2 + \frac{1}{\frac{1}{jX_3}+\frac{4}{Z_{D1}}}\right) \tag{A20}$$

$$X_2 = \sum_{n=3,5,7,\cdots}^{\infty}\frac{\omega\mu_0 b'}{a\Gamma_n}\sin\left(\frac{n\pi d_1}{a}\right)\sin\left\{\frac{n\pi(d_1+r)}{a}\right\} \tag{A21}$$

$$X_3 = \sum_{n=2,4,6,\cdots}^{\infty}\frac{\omega\mu_0 b'}{a\Gamma_n}\sin\left(\frac{n\pi d_1}{a}\right)\sin\left\{\frac{n\pi(d_1+r)}{a}\right\} \tag{A22}$$

$$m^2 = \frac{a}{2b}\csc^2\left(\frac{\pi d_1}{a}\right) \tag{A23}$$

$$Z_1 = \frac{Z}{m^2}. \tag{A24}$$

From (A20), the equivalent circuit is obtained.

References

[1] T. S. Chen, "Characteristics of waveguide resonant irises filters," *IEEE Trans. Microwave Theory Tech.*, vol. MTT-15, p. 260, Apr. 1967.

[2] S. Toyoda and M. Ozasa, "Rectangular waveguide type variable band-pass filters," in *Proc. 1979 IEEE-MTT-S Int. Microwave Symp.*, pp. 281–284, May 1979.

[3] S. Toyoda, "Microstrip variable band-pass filters using varactor-diodes," in *Proc. 1980 IEEE-MTT-S Int. Microwave Symp.*, pp. 153–155, May 1980.

[4] S. Toyoda, "Variable band-pass filter using varactor-diodes," *Trans. IECEJ*, vol. B 61, pp. 1–6, July 1977.

[5] N. Marcuvitz, *Waveguide Handbook*, (MIT Rad. Lab. Ser.), vol. 10. New York: McGraw-Hill, 1951, ch. 6, pp. 353–355.

[6] L. Lewin, *Advanced Theory of Waveguides*. London: Iliffe, 1951, ch. 2, pp. 23–27.